Role of interfacial structure on exchange-biased FeF_2-Fe

J. Nogués,* T. J. Moran,† D. Lederman,‡ and Ivan K. Schuller
Physics Department 0319, University of California–San Diego, La Jolla, California 92093-0319

K. V. Rao
Department of Condensed Matter Physics, Royal Institute of Technology, 10044 Stockholm, Sweden
(Received 10 April 1998; revised manuscript received 6 October 1998)

We have studied the effect of the interface structure on the exchange bias in the FeF_2-Fe system, for FeF_2 bulk single crystals or thin films. The exchange bias depends very strongly on the crystalline orientation of the antiferromagnet for both films and crystals. However, the interface roughness seems to have a strong effect mainly on the film systems. These results indicate that the exchange bias depends strongly on the spin structure at the interface, especially on the angle between the ferromagnetic and antiferromagnetic spins. We have also found a strong dependence of the hysteresis loops shape on the cooling field direction with respect to the antiferromagnetic anisotropy axis, induced by a rotation of the ferromagnetic easy axis as the sample is cooled through T_N. For the single crystal systems the results imply the existence of a perpendicular coupling between the antiferromagnetic and ferromagnetic spins at low temperatures. [S0163-1829(99)02610-7]

I. INTRODUCTION

Exchange bias (H_E) is the shift of the ferromagnetic hysteresis loop away from H=0 due to a unidirectional anisotropy. This anisotropy is caused by the exchange coupling at the interface between a ferromagnetic (FM) and an antiferromagnetic (AF) material after the sample is cooled in a magnetic field through the Néel temperature of the AF.[1] Although this phenomenon was first studied, in 1956, in small ferromagnetic particles embedded in their native antiferromagnetic oxide,[2] it has also been observed in inhomogeneous bulk materials[3] and thin films.[4–17] However, experimentally it is convenient to study exchange anisotropy in a layered form, where it is possible to grow structures of controllable microstructural geometry, especially at the interface. Among the most intensively studied systems are oxide antiferromagnets [CoO,[4–6] NiO,[4,7,8] FeO,[9] Fe_2O_3,[10] and metallic antiferromagnets ($Fe_{50}Mn_{50}$,[8,11–13] $Ni_{50}Mn_{50}$,[8,14] or other metallic systems[15]), with more limited research in sulfides such as FeS,[16] and ferrimagnets.[17] This property has motivated practical industrial applications in magnetoresistive heads as domain stabilizers[12] or in ''spin-valve'' based devices.[13]

Due to the interface nature of the exchange bias, H_E is expected to depend strongly on the AF-FM interface structure, such as the crystalline orientation or the interface disorder, among other factors. However, these kind of experimental studies have been complicated so far by multiphase or polycrystalline AF samples. Moreover, complex spin structures or cubic anisotropy also complicate the analysis of the results. In order to overcome some of these problems we have chosen FeF_2 as the antiferromagnet, because of its simple crystal structure (body centered tetragonal[18]), simple spin structure[19] (see Fig. 1), and its strong uniaxial magnetic anisotropy.[20]

This paper is organized as follows. After the Introduction (Sec. I), the samples are described in a sample preparation (Sec. II) and sample characterization (Sec. III) sections divided in to film (A) and crystals (B). Following these sections, the effect of different structural and measurement parameters: crystalline orientation (Sec. IV), interface disorder (Sec. V) and cooling field direction (Sec. VI) are discussed for films (A) and crystals (B). Finally, the results are analyzed in the Discussion (Sec. VII) and summarized in the

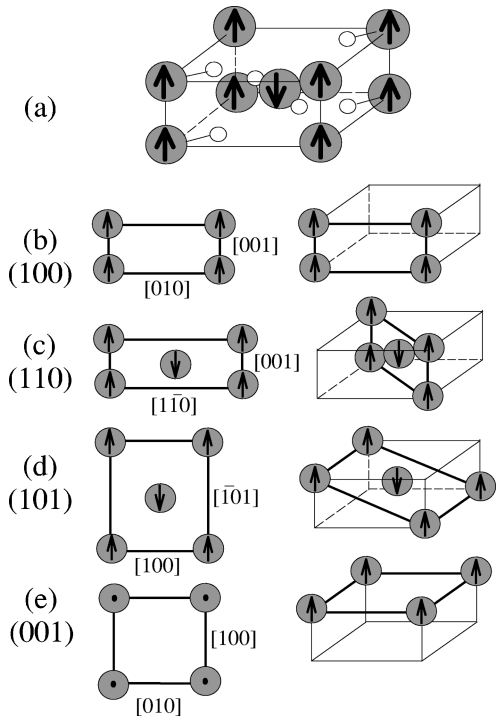

FIG. 1. (a) Bulk FeF_2 spin and crystal structure (Ref. 19). (b) Bulk FeF_2(100) surface spin structure. (c) Bulk FeF_2(110) surface spin structure. (d) Bulk FeF_2(101) surface spin structure (note that the spins are 55° out of the film plane). (e) Bulk FeF_2(001) surface spin structure, where ○ represent Fe^{+2} ions and ◦ represent F^- ions. The lattice is body-centered tetragonal with $a=b=4.697$ Å and $c=3.309$ Å. The arrows represent the magnetic ordering at low temperatures.

Conclusions (Sec. VIII). The results demonstrate the strong dependence of the exchange bias on orientation, for both FeF_2 films and crystals. However, the crystals (roughness, $\sigma \sim 0.5$–200 nm) are less sensitive to interface disorder than the films (roughness, $\sigma \sim 0.5$–5 nm). Furthermore, the dependence of the hysteresis loops on the direction of the cooling field indicates a rotation of the FM easy axis below T_N for both films and crystals.

II. SAMPLE PREPARATION

A. Films

The FeF_2-Fe films were grown on MgO (100), $Al_2O_3(1\bar{1}02)$ (r-plane sapphire), and $Al_2O_3(10\bar{1}0)$ (m-plane, 90°, sapphire) substrates. Typically 90 nm of FeF_2 were deposited by using an electron gun, at a rate of 0.2 nm/s. The substrates were heated to 450°C for 15 min prior to deposition and then cooled to the FeF_2 growth temperature. During the growth of the FeF_2 layer, the substrates were kept at different temperatures, $T_S = 200$–300°C, in order to control the interface roughness.[21] Following the FeF_2 deposition, a 13 nm Fe layer, at a rate of 0.1 nm/s, at $T_S = 150$ °C was electron beam evaporated. In order to protect the FeF_2-Fe bilayer, a 9 nm capping layer of silver was deposited, at a rate 0.05 nm/s, at $T_S = 150$ °C using a Knudsen cell. The base pressure of the chamber was better than 1×10^{-7} Torr and the pressure during deposition was lower than 2×10^{-6} Torr. The thickness of the different layers was controlled by a calibrated quartz oscillator.

B. Single crystals

The FeF_2 single crystal was grown using the Bridgeman-Stockbarger method. It was aligned using a Laue x-ray camera and cut with a diamond wire into three different orientations (001), (110), and (100).

To control the surface roughness the crystals were subjected to one of two possible surface treatments: (1) sanding with 400 grit sand paper followed by *in situ* ion bombarded with 5 kV Ar ions for 30 min, (2) fine polishing with 6 and 1 μm powder steps. After surface treatment, the crystals were transferred into a Riber ultra high vacuum molecular beam epitaxy (MBE) system (2×10^{-10} Torr base pressure). The polished crystals were subject to an additional annealing treatment, in vacuum, at 400 °C for 30 min to improve surface quality. One sample with polished interfaces was damaged *in situ* with ion bombardment, using 5 kV Ar ions for 30 min, in order to obtain an interface with moderate roughness. 20 nm of Fe were deposited onto the FeF_2 single crystals at $T_S = 150$ °C using electron beam evaporation, at a rate of 0.1 nm/s. To protect the Fe layer, a 20 nm silver capping layer was deposited, at a rate 0.05 nm/s, at room temperature using a Knudsen cell. During a typical deposition the pressure was lower than 5×10^{-9} Torr. Deposition rates were controlled using electron impact emission spectroscopy.

III. SAMPLE CHARACTERIZATION

A. Films

Structural characterization of the films was carried out by *ex situ* x-ray diffraction using Cu-K_α radiation ($\lambda = 0.15418$ nm). Both high angle θ-2θ scans and rocking curves were measured. θ-2θ scans (Fig. 2) imply that under the above conditions the different FeF_2 layers grow in the (110), (101), and (001) orientations on MgO (100), $Al_2O_3(1\bar{1}02)$, and $Al_2O_3(10\bar{1}0)$ substrates, respectively. We found no substrate which rendered single phase (100) FeF_2 films. The full width at half maximum of the rocking curves of the different FeF_2 orientations peaks were $\Delta\theta = 0.9° - 1.7°$(110), $\Delta\theta = 0.4° - 0.7°$(101), and $\Delta\theta = 0.4° - 0.6°$(002), samples grown at the higher substrate temperatures had narrower rocking curves. The sample grown on $Al_2O_3(10\bar{1}0)$ at $T_S = 200$ °C contained both (001) and (110) orientations, and was thus discarded from this study. The Fe layers were polycrystalline mainly in the (110) and (100) orientations, with rocking curve widths larger than 4°, for all samples.

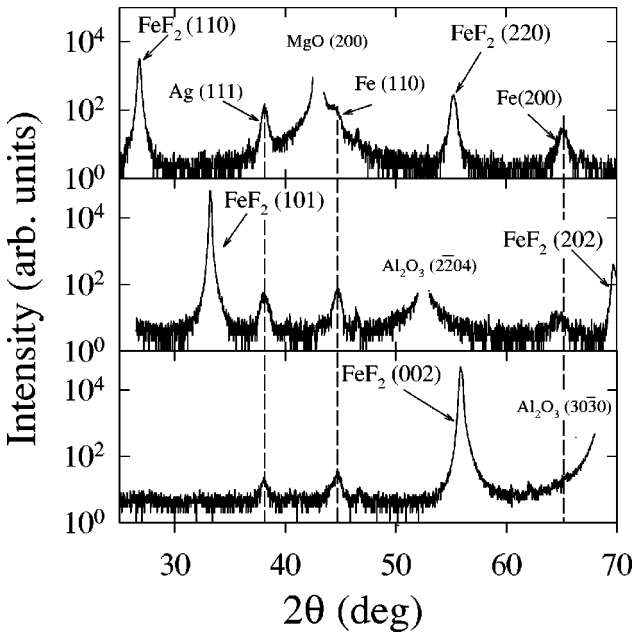

FIG. 2. High-angle x-ray diffraction ($\lambda = 0.15418$ nm) for (a) FeF_2(110)(~90 nm)-Fe(~13 nm)-Ag(~9 nm) grown at 200 °C on MgO(100), (b) FeF_2(101)(~90 nm)-Fe(~13 nm)-Ag(~9 nm) grown at 250 °C on $Al_2O_3(1\bar{1}02)$, and (c) FeF_2(001) (~90 nm)-Fe(~13 nm)-Ag(~9 nm) grown at 300 °C on $Al_2O_3(10\bar{1}0)$.

Grazing incidence x-ray diffraction was used to investigate the antiferromagnetic layers structure in the film plane. In this study, the detector angle 2θ was set to one of the FeF_2 in-plane reflections, with the x rays almost parallel to the plane of the film. The sample was then rotated about its normal. The results, shown in Fig. 3, imply that all the samples were oriented in the plane. However, the (110) samples, with a rectangular unit cell on a substrate with square symmetry in the plane, show a fourfold symmetry, indicating that these samples are twinned in the plane. Note that the two in plane peaks in the FeF_2(001) are not exactly at 90°, probably due to different film-substrate mismatch in different in-plane directions. The epitaxial relations are listed in Table I.

To evaluate the interface roughness, specular small angle x-ray diffraction was carried out. We found that the interface

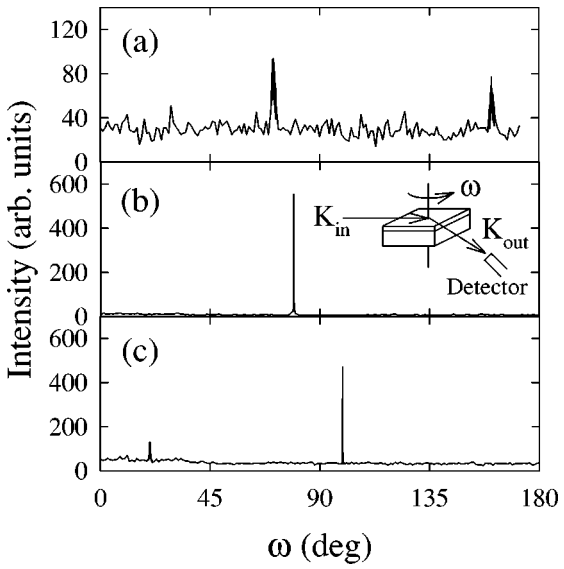

FIG. 3. In-plane x-ray scattering for ($\lambda = 0.15418$ nm) for (a) the [002] in-plane peak for $FeF_2(110)(\sim 90$ nm)-Fe (~ 13 nm)-Ag(~ 9 nm) grown at 200 °C on MgO(100), (b) the [200] in-plane peak for $FeF_2(101)(\sim 90$ nm)-Fe(~ 13 nm)-Ag (~ 9 nm) grown at 250 °C on $Al_2O_3(1\bar{1}02)$, and (c) the [200] in-plane peak for $FeF_2(001)(\sim 90$ nm)-Fe(~ 13 nm)-Ag (~ 9 nm) grown at 300 °C on $Al_2O_3(10\bar{1}0)$. Shown in the inset is the measurement geometry.

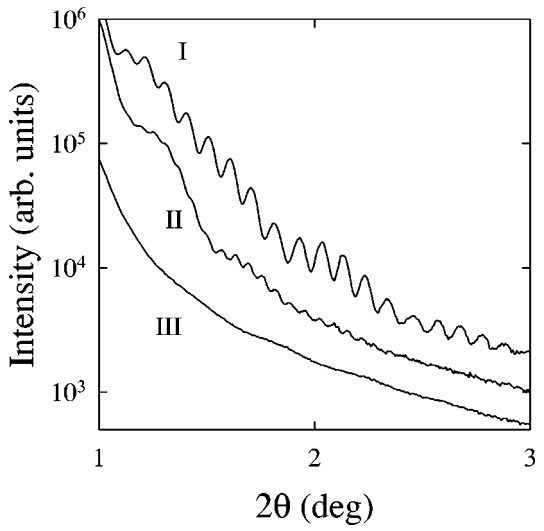

FIG. 4. Small angle x-ray diffraction ($\lambda = 0.15418$ nm) for $FeF_2(101)(\sim 90$ nm)-Fe(~ 13 nm)-Ag(~ 9 nm) samples with the FeF_2 grown at different substrate temperatures, $T_S = 200$ °C (I), $T_S = 250$ °C (II), $T_S = 300$ °C (III).

roughness increases with the FeF_2 growth temperature. For the samples grown on MgO (100), a quantitative analysis was performed using the SUPREX program's[22] low-angle recursive optical model[23] adapted for trilayers. Using this approach interface rms roughness values in the range $\sigma \sim 0.5$–5 nm were obtained.[21] As found for the (110) orientation, higher FeF_2 deposition temperatures for the (101) and (001) orientations also result in lower amplitudes of the high frequency peaks (Fig. 4), which implies increased thickness fluctuations and therefore an enhanced FeF_2 surface roughness.

To investigate further the surface of the FeF_2 layers, single FeF_2 films were grown on MgO(100) under the same conditions. The surface structure of these films was studied, using *ex situ* diffuse x-ray scattering, atomic force microscopy (AFM), and reflection high energy electron diffraction (RHEED). The diffuse x-ray scattering was analyzed using a model based on the Born approximation.[24] The roughness obtained from the diffuse x-ray scattering and the AFM (Fig. 5) showed the same trend as the specular x-ray scattering of the bilayers, i.e., the roughness increases as the substrate temperature is increased.[21] This trend is similar to previously reported AFM data for ZnF_2 homoepitaxial films.[25] Moreover, the lateral correlation length of the vertical roughness, as obtained from diffuse x-ray scattering and AFM, also increases with substrate temperature.[21] Finally, only the single FeF_2 film sample grown at $T_S = 200$ °C displayed two-dimensional RHEED patterns, indicating a more ordered surface.

The magnetic characterization was carried out using a SQUID magnetometer. The samples were cooled from 300 K, i.e., above T_N (FeF_2) = 78.4 K, to 10 K in the presence of a magnetic field H_{fc}, in the plane of the film. H_{fc} was large enough to saturate the FM layer (e.g., $H_{sat} = 200$ Oe

TABLE I. Epitaxial relations for thin films.

Crystalline orientation	Epitaxial relationship	Lattice mismatch %
$FeF_2(110)$	$FeF_2\langle 001\rangle \| MgO\langle 110\rangle$	11
	$FeF_2\langle \bar{1}10\rangle \| MgO\langle \bar{1}10\rangle$	11
$FeF_2(101)$	$FeF_2\langle 100\rangle \| Al_2O_3\langle 11\bar{2}0\rangle$	1
	$FeF_2\langle \bar{1}01\rangle \| Al_2O_3\langle \bar{1}101\rangle$	10
$FeF_2(001)$	$FeF_2\langle 100\rangle \| Al_2O_3\langle 0001\rangle$	8
	$FeF_2\langle 010\rangle \| Al_2O_3\langle 1\bar{2}10\rangle$	1

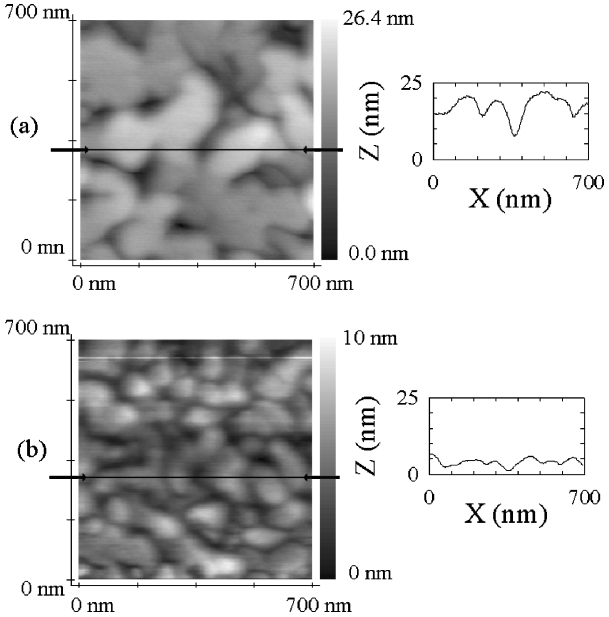

FIG. 5. Top view atomic force microscopy images and line scans of single $FeF_2(110)(\sim 90$ nm) films grown at (a) $T_S = 200$ and (b) $T_S = 300$ °C.

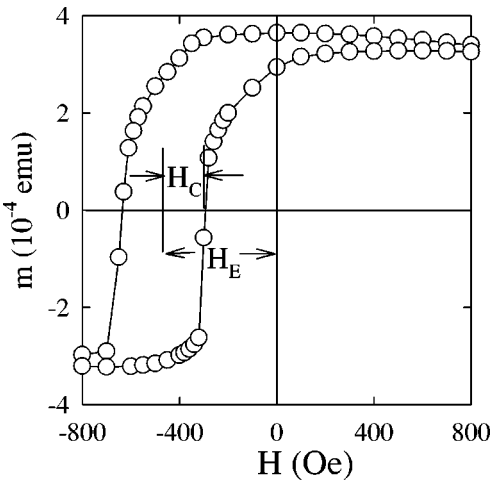

FIG. 6. Hysteresis loop at $T=10$ K for $FeF_2(110)$ ($\sim$90 nm)-Fe($\sim$13 nm)-Ag($\sim$9 nm) grown at 200 °C on MgO(100). The definitions for the exchange bias (H_E) and coercivity (H_C) are also shown.

for $t_{FM}=13$ nm). Afterwards, hysteresis loops were measured for $-H_{fc}<H<H_{fc}$, typically every 10 up to 110 K. Figure 6 shows a typical hysteresis loop exhibiting a large shift H_E and coercivity H_C, as indicated in the figure. To study the effects of the field cooling direction, samples (about 5 mm in size) were manually rotated for each angle Φ, with respect to the field and positioned in the sample holder. Due to the small size of the sample, this rotation was somewhat inaccurate, resulting in large error bars. The measurements were carried out for angles between the filed cooling and AF anisotropy axes between 0–90°, where both clockwise ($+\Phi$) and counterclockwise ($-\Phi$) rotations were performed.

B. Single crystals

The structure of the FeF_2 single crystals covered with an Fe layer was determined from *ex situ* x-ray diffraction (high angle θ-2θ scans and rocking curves) using Cu-K_α radiation ($\lambda=0.15418$ nm). θ-2θ scans confirmed the orientations of the different FeF_2 crystals to be (110), (100), and (001). Due to the size, shape, and growth direction of the FeF_2 single crystal it was difficult to obtain large enough samples in the (101) direction. The full width at half maximum of the rocking curves of the different FeF_2 orientations were typically $\Delta\theta<0.1°$. The Fe films grown on polished and annealed (110) and (100) FeF_2 crystals, exhibit mainly (110) orientation, with typical rocking curve widths $\Delta\theta\simeq4°$. The Fe films grown on polished and annealed (001) crystals and all the samples grown on sanded crystals were polycrystalline mainly with Fe (110) and (100) orientations.

The disorder of the FeF_2 crystals surface was investigated by *in situ* RHEED. The sanded crystals did not exhibit any RHEED patterns. The polished crystals showed two-dimensional diffraction RHEED patterns, which became sharper upon annealing, indicating that annealing improves the crystalline ordering.[26] After the polished and annealed samples were ion bombarded the spots on the RHEED pattern became broader implying a deterioration of the surface. Unfortunately, RHEED patterns do not allow for simple quantitative roughness analyses. RHEED was also carried out on the Fe films after deposition. The Fe films grown on the polished and annealed (110) and (100) crystals showed ''spotty'' RHEED patterns, indicating that these films were oriented in the plane.

TABLE II. Epitaxial relations for single crystals.

Crystalline orientation	Epitaxial relationship	Lattice mismatch %
$FeF_2(110)$	$FeF_2\langle001\rangle\|\|Fe\langle001\rangle$	15
	$FeF_2\langle\bar{1}10\rangle\|\|Fe\langle\bar{1}10\rangle$	42
$FeF_2(100)$	$FeF_2\langle001\rangle\|\|Fe\langle001\rangle$	15
	$FeF_2\langle\bar{1}00\rangle\|\|Fe\langle\bar{1}10\rangle$	16

The in-plane orientation of the ferromagnetic layers with respect to the antiferromagnetic substrate was also confirmed by off-specular x-ray diffraction. Measurements were taken with the scattering vector at 27° from the growth direction to detect the Fe (310) peaks and FeF_2 (510) peaks. By comparing the azimuthal variation in the intensity of these peaks, we determined that the Fe[001] direction was primarily parallel to the FeF_2[001] direction.[26] The epitaxial relations for these are listed in Table II.

To quantify the length scale of the roughness of the sanded crystals, profilometry (Dektak) studies were carried out, where roughness values in the range of a few hundred nm were usually obtained. The magnetic characterization of the crystals was similar to the one used for the FeF_2 films. However, the hysteresis loops of the crystals had a large linear background due to the susceptibility of the FeF_2 crystals, which was subtracted from the data in order to clearly observe the FM hysteresis loops.[26] A temperature dependent offset of the magnetization, on the order of 2×10^{-3} emu/g, due to FeF_2 piezomagnetism,[27] was also subtracted.[26]

IV. DEPENDENCE OF H_E ON THE AF CRYSTALLINE ORIENTATION

A. Films

The temperature dependence of H_E for the samples for the three film orientations (110), (101), (001), grown at $T_S=300$ °C, is shown in Fig. 7. The exchange bias behaves differently for the three orientations, with the (110) orientation having the largest exchange bias, followed by the (101) orientation, and finally the (001) orientation having the smallest exchange bias. We also found that this general trend is independent of growth temperature (i.e., the roughness), as can be seen in the inset of Fig. 7. The different spin configurations for the different orientations (Fig. 1), differ in the angle between the spins and the interface plane, i.e., the (110) orientation has 0°, the (101) orientation has 55°, and the (001) orientation has 90°. This fact suggests two possible qualitative explanations for the observed behavior.

The exchange bias Hamiltonian contains a term which accounts for the coupling at the interface

$$H_{\rm int}=J_{\rm int}\bar{S}_{\rm AF}\bar{S}_{\rm FM}, \tag{1}$$

where $J_{\rm int}$ is the exchange at the interface, $S_{\rm AF}$ and $S_{\rm FM}$ are the antiferromagnetic and ferromagnetic spins at the inter-

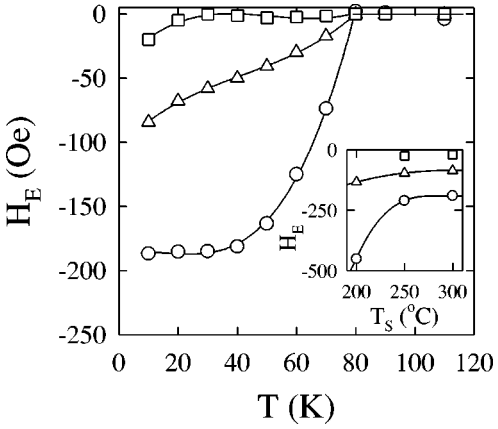

FIG. 7. Temperature dependence of the exchange bias H_E for $FeF_2(110)$(~90 nm)-Fe(~13 nm)-Ag(~9 nm) on MgO(100) (○), $FeF_2(101)$(~90 nm)-Fe(~13 nm)-Ag(~9nm) on $Al_2O_3(1\bar{1}02)$ (△), and $FeF_2(001)$(~90 nm)-Fe(~13 nm)-Ag (~9 nm) on $Al_2O_3(10\bar{1}0)$ (□), grown at $T_S = 300$ °C. The inset shows the dependence of the exchange bias H_E at $T = 10$ K for the three orientations with respect to the substrate temperature T_S. The lines are a guide to the eye.

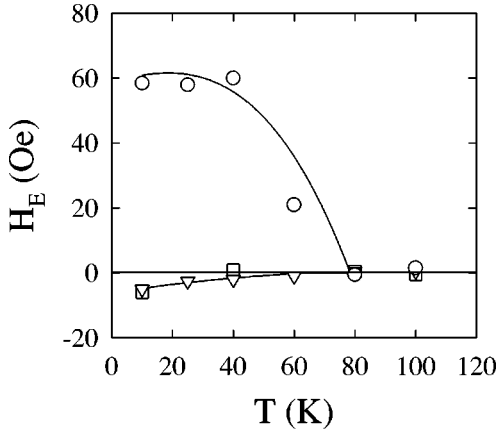

FIG. 8. Temperature dependence of the exchange bias H_E for the Fe(~20 nm)-Ag(~20 nm) grown on the (001) (□), (100) (▽), and (110) (○) FeF_2 polished-annealed crystals. The (001) crystal is field cooled along the [100] direction while the (100) and (110) crystals were field cooled along the AF anisotropy axis [001]. The lines are a guide to the eye.

face, respectively. Assuming that the AF spins at the interface remain in their bulk orientation because of the strong FeF_2 uniaxial anisotropy, and that the FM spins are parallel to the interface due to shape anisotropy, the exchange bias should have a term proportional to

$$H_E \propto J_{\text{int}} |S_{\text{AF}}||S_{\text{FM}}| \cos\alpha, \tag{2}$$

where α is the angle between the AF spins and FM spins at the interface. Thus, the (110) orientation, with $\alpha = 0°$, should have the maximum exchange bias, the (101) orientation, with $\alpha = 55°$, should have exchange bias about half of that of (110), and finally the (001) orientation, with $\alpha = 90°$, should not have any exchange bias. This simple model agrees qualitatively with the experimental results (Fig. 7).

Another possible explanation assumes that the dominant factor in H_E is AF domain formation. Therefore, following some of the exchange bias models[28,29]

$$H_E \propto \sqrt{K_{\text{AF}} A_{\text{AF}}}. \tag{3}$$

Thus in the case of out-of-plane AF spins, the effective AF in-plane anisotropy K_{eff}, and stiffness A_{eff}, would play a major role. Due to the angle of the AF spins, the effective anisotropy and stiffness at the interface plane should scale with $\cos\alpha$, thus

$$H_E \propto \sqrt{K_{\text{eff}} A_{\text{eff}}} = \sqrt{K_{\text{AF}} A_{\text{AF}}} \cos\alpha, \tag{4}$$

leading to the same conclusions as above.

These phenomenological descriptions may, to some extent, also account for the variations in exchange bias found in different FeMn orientations for $FeMn/Fe_{20}Ni_{80}$ bilayers,[11] where the spins at the interfaces for the different AF orientations have different AF-FM spin coupling angles. In the case of the antiferromagnets NiO and CoO the analysis is more complicated because for a given crystalline orientation the spins can have four different directions on the plane due to the cubic anisotropy in these materials.[6]

Other mechanisms could explain the results. These include differences in lattice matching between the Fe and the FeF_2 unit cells, different AF domain configurations, and different AF microstructures. The small exchange bias for the (001) orientation can be due to several factors, such as the different lattice match of the FeF_2 film with the substrate in the different directions, which could result in a distorted unit cell, interface roughness, which would cause small amounts of other orientations to be present at the interface, the crystallinity of the sample which would cause some areas of the interface to have slightly different angles with the interface plane, or some residual oxidation of the Fe layer. (Note that oxidation should also affect other orientations, however, the effect would be a smaller fraction of the total H_E).

It is important to note that both (110) and (101) directions are *spin compensated* in the plane (see Fig. 1), i.e., both AF sublattices end at the surface. Because of this, compensated surfaces have zero net magnetization in the plane. Therefore, naively one would expect these kind of surfaces to have zero exchange bias. However, we observe very large shifts for both spin compensated orientations. Large exchange bias for nominally compensated AF spins has been observed in several systems, e.g., $FeMn/Fe_{20}Ni_{80}$,[11] $CoO/Fe_{20}Ni_{80}$,[6] or CoO/Fe_3O_4.[5]

B. Single crystals

The temperature dependence of H_E for the three polished and annealed crystals is shown in Fig. 8. As in the film samples, the (001) surface has a very small exchange bias, as expected from the AF and FM spin orientations being at 90° from each other. However, the results for the (100) and (110) orientations are rather puzzling. The (100) orientation, with *uncompensated* spins at the interface (see Fig. 1) exhibits virtually no exchange bias, contrary to what would be expected from simple models.[2] Furthermore, the (110) orientation, with *compensated* spins at the surface (see Fig. 1), shows a shift of the FM loop towards positive fields when

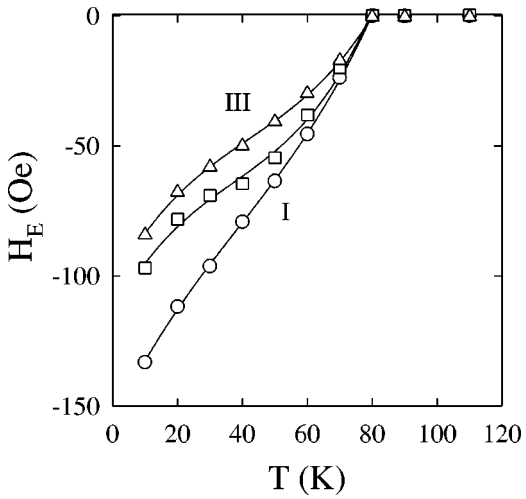

FIG. 9. Temperature dependence of the exchange bias H_E when field cooled along the AF $[\bar{1}01]$ axis, for $FeF_2(101)$ (~90 nm)-Fe(~13 nm)-Ag(~9 nm) samples with the FeF_2 grown at different substrate temperatures $T_S=200$ °C (I, ○), $T_S=250$ °C (II, □), $T_S=300$ °C (III, △). The lines are a guide to the eye.

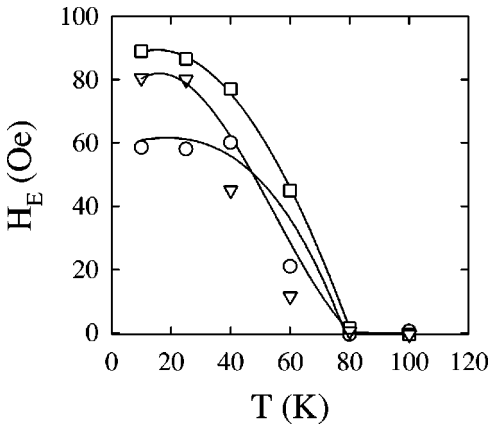

FIG. 10. Temperature dependence of the exchange bias H_E for Fe(~20 nm)-Ag(~20 nm) grown on (110) FeF_2 polished (○), polished-bombarded (∇), and sanded (□) crystals, field cooled along the AF anisotropy axis [001]. The lines are a guide to the eye.

cooled in a 2000 Oe positive field, contrary to what is normally observed, and expected from simple models.[2] This is similar to the exchange bias observed in FeF_2/Fe bilayers cooled in large fields.[30]

V. DEPENDENCE OF H_E ON THE INTERFACE DISORDER

A. Films

The results for the $FeF_2(110)$ films grown on MgO(100) have been published elsewhere.[21] The main conclusions are that (a) H_E decreases with increasing roughness ($\sigma \sim 0.5$–5 nm) and that (b) H_E decreases with increasing lateral correlation length of the vertical roughness.[21]

Figure 9 shows that H_E decreases as the surface roughness (characterized in Fig. 4) for $FeF_2(101)$ increases, as observed for $FeF_2(110)$. The analysis of the exchange bias for this orientation is more complicated than for the $FeF_2(110)$ orientation, due to its strong dependence on the in-plane cooling field direction, as discussed in Sec. VI A. The results shown in Fig. 9 are for samples cooled along the AF anisotropy axis projection on the (101) plane, i.e., the $[\bar{1}01]$ direction. Note that the effect of lateral correlation length has not been studied for the $FeF_2(101)$ films. Finally, the $FeF_2(001)$ orientation exhibits virtually no dependence of the exchange bias on interface roughness ($H_E \approx 0$) for the two substrate temperatures ($T_S=250,300$ °C) for which pure (001) films are obtained.

B. Single crystals

Contrary to what is observed in the films and $Fe_{20}Ni_{80}$/CoO single crystals,[6] H_E in Fe/FeF_2 single crystals depends weakly on interface roughness ($\sigma \sim 0.5$–200 nm). The exchange bias for the (100) and (001) orientations samples remains unchanged, independently of the surface treatment with no exchange bias ($H_E \approx 0$). As shown in Fig. 10, the (110) orientation crystals, cooled along the [001] direction, become slightly less ''positive'' (by about 40 %) as the quality of the surface improves (from sanded to polished annealed). This trend is in agreement with the results for (110) films which have larger (more negative) exchange bias for smoother interfaces.[21] These results are also consistent with the results obtained for $Fe_{20}Ni_{80}$/CoO single crystals,[6] in the sense that the *magnitude* of H_E increases with increasing roughness.

VI. DEPENDENCE OF HYSTERESIS LOOPS ON THE COOLING FIELD DIRECTION: NONCOLLINEAR COUPLING

A. Films

The magnetic properties of the (110) films exhibit only a weak angular dependence, probably due to their twinned nature. When the samples are cooled along the [001]-$[\bar{1}10]$ twin (perpendicular or parallel to the AF anisotropy axis) H_E is about 20% smaller than when cooled along the $[\bar{1}\bar{1}2]$-$[11\bar{2}]$ twin ($-45°$ or $+45°$ to the AF anisotropy axis). The comparison between the shapes of the hysteresis curves measured at room temperature and at 10 K hysteresis loops (remanence increase for the $\pm 45°$ between room temperature and 10 K and vice versa for [001]-$[\bar{1}10]$, although no major changes are observed in the coercivity) could imply that the direction of the FM easy axis changes when cooling through T_N. However, due to the twinned nature of $FeF_2(110)$ films, it is difficult to analyze these results in more detail.[30] The (001) samples exhibit virtually no angular dependence because the spins of the FeF_2 are perpendicular to the interface.

The exchange bias for the $FeF_2(101)$ orientation has a strong dependence on the cooling field direction (Fig. 11). The dependence of H_E on the cooling angle is different for films grown at different temperatures. The roughest sample

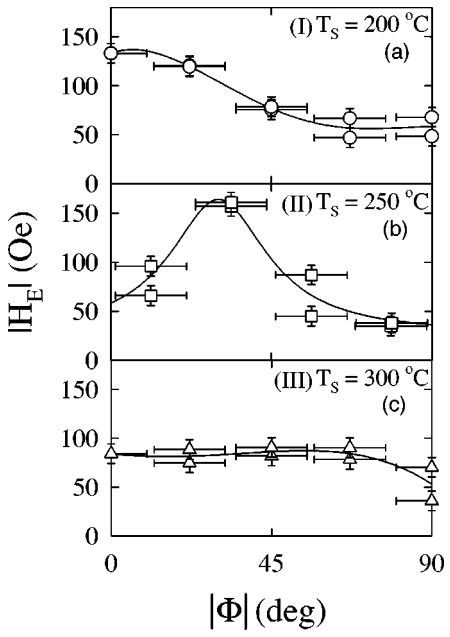

FIG. 11. Dependence of the absolute value of the exchange bias H_E, on the absolute value of the angle Φ between the cooling field and the AF anisotropy axis for $FeF_2(101)(\sim 90$ nm)-Fe (~ 13 nm)-Ag(~ 9 nm) samples with the FeF_2 grown at different substrate temperatures, (a) $T_S = 200$ °C (I, ○), (b) $T_S = 250$ °C (II, □), (c) $T_S = 300$ °C (III, △). Note that $+\Phi$ and $-\Phi$ results are shown for each angle. The lines are a guide to the eye.

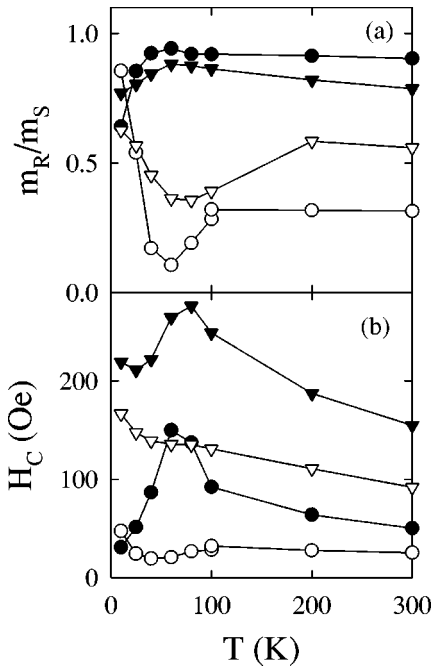

FIG. 12. Temperature dependence of (a) the reduced remanence m_R/m_S and (b) the coercivity for Fe(~ 20 nm)-Ag(~ 20 nm) grown on the $FeF_2(110)$ polished and annealed crystal (○) and sanded crystal (▽) field-cooled parallel (open symbols) and perpendicular (filled symbols) to the $FeF_2[001]$. The lines are a guide to the eye.

has only a weak angular dependence, the sample grown at $T_S = 250$ °C has a peak, and the smoothest sample has a steplike behavior.

From the shapes of the hysteresis loops measured at different temperatures and cooling angles (the remanence and coercivity decrease at low temperatures for the room temperature easy axis direction and viceversa for the room temperature hard axis), it appears that the FM easy axis changes its direction below the Néel transition of the AF. However, from the present data it is difficult to estimate the magnitude of this rotation. The fact that the FM and AF anisotropy axes are at an angle from each other (not parallel, as usually assumed) can qualitatively explain the observed dependence of H_E on the cooling field direction. The equilibrium position of the interfacial spins, and thus the observed exchange bias, is the result of a trade off between the strength of AF and FM anisotropies and the strength of the coupling at the interface. The dependence of H_E on the cooling field direction similar to the experimental ones can be obtained if the hysteresis loops are computed taking into account the noncollinearity of the FM and AF spins.[31]

B. Single crystals

For the $FeF_2(001)$ orientation, H_E remains unchanged when field-cooling along the [010] or [100] directions, as expected from the spin orientation (perpendicular to the interface plane) and found in the film samples.

The $FeF_2(110)$ samples exhibit a ''small'' (when compared with the film systems) *positive* H_E when field cooled parallel to the AF axis ([001]) but almost no shift when field-cooled perpendicular ($[1\bar{1}0]$) to it. On the other hand, for the $FeF_2(100)$ samples $H_E \sim 0$, independently of the field cooling direction ([001], [010]).

However, as reported elsewhere[32] the shape, coercivity and remanence of the hysteresis loops provides clues for understanding the behavior of this system. Briefly, from the hysteresis loops of the $FeF_2(110)$ and $FeF_2(100)$ crystals, we can infer that at room temperature the easy axis of the FM is parallel to the [001] axis of the FeF_2. However, at $T = 10$ K, the easy axis of the FM is perpendicular to the [001] axis of the FeF_2, i.e., the FM easy axis has rotated 90°. Thus at low temperatures the AF and FM spins at the interface are coupled *perpendicular* to each other. The temperature dependence of the remanence and coercivity (Fig. 12), implies that the rotation starts near T_N, indicating that it is the ordering of the AF spins that drives the change in the FM anisotropy direction. The (110) and (100) single crystal samples with different roughness (sanded, ion bombarded, and polished) exhibit the same trend, but it is more pronounced in the polished crystal samples (Fig. 12). As mentioned above, a similar FM easy axis rotation has also been observed in the $FeF_2(110)$ and $FeF_2(101)$ films. Similar perpendicular coupling has been observed in $FeMn/Fe_{20}Ni_{80}$,[11] $CoO/Fe_{20}Ni_{80}$ single crystal systems[6], CoO/Fe_3O_4 multilayer systems,[33] and CoO/Co.[34] However, in CoO/Fe_3O_4 it appears that the CoO AF spins are the ones which rotate in order to achieve a perpendicular coupling[33].

This behavior indicates that as the AF orders it becomes advantageous for the FM and AF spins to point perpendicular to each other. This can be intuitively understood in the (110) case, where the spins are assumed to conserve the bulk

TABLE III. Summary of exchange bias properties for FeF_2 films and single crystals.

	Spin direction	Compensated vs. uncompensated	H_E	Roughness dependence of $\lvert H_E \rvert$
[110]				
Films	0°	Compensated	Large	Decrease
Crystals	0°	Compensated	Small	Increase
[101]				
Films	55°	Compensated	Moderate	Decrease
Crystals				
[001]				
Films	90°	Uncompensated	Zero	Unchanged
Crystals	90°	Uncompensated	Zero	Unchanged
[100]				
Films				
Crystals	0°	Uncompensated	Zero	Unchanged

orientation, i.e., compensated at the interface. In this case, it would be energetically costly for the FM to maintain its spins parallel to one AF spin sublattice but antiparallel to the other sublattice, thus it may be energetically favorable for the FM to rotate perpendicular to both AF sublattices. This reasoning can be extended to the uncompensated (100) orientation if because of defects (e.g., roughness or domain formation), both sublattices are exposed at the interface with the ferromagnet. The perpendicular coupling between AF and FM layers is consistent with recent micromagnetic calculations.[35] This model can explain many of the observed results in the FeF_2/Fe system, such as the existence of H_E in compensated surfaces or positive H_E.[35]

However, one cannot rule out that the observed effect could arise due to magnetoelastic effects. The lattice parameters of FeF_2 are known to change non-monotonically near $T=T_N$.[36] One can argue that these changes in lattice parameter can be transferred to the Fe layer, and thus induce a stress anisotropy perpendicular to the anisotropy of the Fe above T_N.[26,32]

VII. DISCUSSION

The properties of FeF_2 crystals and films covered by thin Fe layers are summarized in Table III. The existence of H_E in compensated film surfaces can be explained to some extent by some of the exchange bias models. The following mechanisms for H_E in these surfaces have been proposed: (i) the interfacial energy due to AF domain formation due to random fields created by roughness or other defects,[28] (ii) perpendicular coupling of the AF and FM spins at the interface and AF spin flop,[35] (iii) transfer of the FM spin waves to the AF,[37] (iv) uncompensated AF spins at the interface due to thermoremanent magnetization,[38] or (v) random anisotropy at the interface.[39] Moreover, as discussed earlier,[21] the effects of roughness on the exchange bias in thin films are consistent with models which rely on domain wall formation in the antiferromagnet,[28,29] and other more recent models,[35,37,39] through increased randomness or reduction of the coupling at the interface.

On the other hand, the absence of H_E for most of the single crystal orientations with in-plane interface spins is probably related to the perpendicular coupling at the interface. Intuitively, to observe H_E canting of the AF spins is necessary.[35] Thus, if canting is hindered, e.g., by the large AF anisotropy, H_E should be small. The fact that loop shifts are actually observed for the (110) orientations could be related to structural factors such as worse lattice matching at the FeF_2(110)-Fe(110) interface than at the FeF_2(100)-Fe(110) interface. This mismatch would cause more FM spins not to be perpendicularly coupled to the AF for the FeF_2(110) orientation. The presence of spins not perpendicularly coupled could then cause exchange bias. Note that due to twinning and/or reduced grain size thin films cannot attain perpendicular coupling, thus the mechanism for H_E is probably different. However, one cannot rule out that these effects in FeF_2 crystals could be related to different atomic exchange interactions at the interface or different types of domain formations for the different orientations. Additionally, the positive H_E observed in (110) single crystals can be explained by a reduced effective coupling between FM and the AF spins. If the effective coupling is weaker, smaller cooling fields than for the films would be necessary for the AF to overcome the coupling, so that the top AF spins align parallel with the cooling field instead of coupling to the FM layer, therefore inducing a positive exchange bias.[30]

Finally, the weak dependence of H_E on the interface roughness for the (110), (001), and (100) orientations could be related to the perpendicular coupling at the interface between AF-FM, i.e., as long as the coupling remains perpendicular H_E continues to be small. Another possibility could be that the interfaces for the crystals have different types of defects than the ones in the films, hence the magnetic properties (e.g., domain formation and/or pinning) could be less sensitive to one type of defect. Moreover, due to the large anisotropy in FeF_2 the domain walls will be rather small, thus defects larger than the domain wall thickness should not affect H_E.

VIII. CONCLUSIONS

We have studied the dependence of the exchange bias on the interface structure for the FeF_2-Fe system, for FeF_2 films, and single crystals. The exchange bias for the films is strongly affected by the out-of-plane angle between the AF and FM spins, when AF spins lie on the interface plane the system exhibits maximum H_E whereas for perpendicular spins the system has no H_E. Both orientations (110), (101) with compensated spins exhibit large H_E, contrary to naive expectations. The exchange bias magnitude of the films decreases with increasing roughness. The exchange bias of the crystals is also sensitive to the spin configuration at the interface but some of the results are puzzling: the samples grown on FeF_2(100) crystals with *uncompensated* surfaces do not exhibit any H_E, while the samples grown on the FeF_2(110) *compensated* surface have loop shifts in a direction contrary to what is normally observed in exchange bias

systems or what is expected from simple models. As for the roughness, it only affects slightly the samples which show H_E, while the others remain unchanged.

A feature shared by the film and single crystal samples is the fact that the easy axis of the FM changes its direction at the AF transition temperature. The results for the (110) and (100) crystals clearly indicate that there is a perpendicular coupling between the AF and FM spins at $T=10$ K, in agreement with recent micromagnetic calculations.

Moreover, in both systems the fully compensated surface exhibits the largest exchange bias. Clearly, a very important ingredient in understanding exchange bias is the spin configuration at the interface. Further experimental work such as neutron scattering, magnetic circular dichroism, or the Mössbauer effect regarding the details of the interface spin configuration is needed.

ACKNOWLEDGMENTS

We thank Dr. V. Speriosu for motivating our initial interest in exchange anisotropy and E.D. Dahlberg and H. Suhl for useful conversations. This work was supported by the U. S. Dept. of Energy. J.N. thanks the NATO Scientific Committee and the Spanish Ministerio de Educación y Ciencia for their financial support.

*On leave from the Grup d'Electromagnetisme, Universitat Autònoma de Barcelona, Barcelona, Spain.

†Permanent address: IBM (E44/015), 5600 Cottle Rd., San Jose, CA 95193.

‡Permanent address: Dept. of Physics, West Virginia University, Morgantown, WV 26506-6315.

[1] For a recent review, see J. Nogués and Ivan K. Schuller, J. Magn. Magn. Mater. (to be published).

[2] W.H. Meiklejohn and C.P. Bean, Phys. Rev. **102**, 1413 (1956); **105**, 904 (1957).

[3] K. Tagaya and M. Fukada, J. Phys. Soc. Jpn. **46**, 53 (1979); S. Jin, T.H. Tiefel, E.M. Gyorgy, L.H. Chen, J.V. Waszczak, and G.W. Kammlott, IEEE Trans. Magn. **28**, 3192 (1992).

[4] M.J. Carey and A.E. Berkowitz, Appl. Phys. Lett. **60**, 3060 (1992).

[5] P.J. van der Zaag, R.M. Wolf, A.R. Ball, C. Bordel, L.F. Feiner, and R. Jungblut, J. Magn. Magn. Mater. **148**, 346 (1995).

[6] T.J. Moran, J.M. Gallego, and Ivan K. Schuller J. Appl. Phys. **78**, 1887 (1995); T.J. Moran and Ivan K. Schuller, *ibid.* **79**, 5106 (1996).

[7] R.P Michel, A. Chaiken, Y.K. Kim, and L.E. Johnson, IEEE Trans. Magn. **32**, 4651 (1996); S. Soeya, S. Tadokoro, T. Imagawa, M. Fuyama, and S. Narishige, J. Appl. Phys. **74**, 6297 (1993).

[8] T. Lin, C. Tsang, R.E. Fontana, and J.K. Howard, IEEE Trans. Magn. **31**, 2585 (1995).

[9] D.V. Dimitrov, A.S. Murthy, G.C. Hadjipanayis, and C.P. Swann, J. Appl. Phys. **79**, 5106 (1996).

[10] N. Hasegawa, A. Makino, F. Koike, and K. Ikarashi, IEEE Trans. Magn. **32**, 4618 (1996).

[11] R. Jungblut, R. Coehoorn, M.T. Johnson, J. aan de Stegge, and A. Reinders, J. Appl. Phys. **75**, 6659 (1994); R. Jungblut, R. Coehoorn, M.T. Johnson, Ch. Sauer, P.J. van der Zaag, A.R. Ball, T.G.S.M. Rijks, J. aan de Stegge, and A. Reinders, J. Magn. Magn. Mater. **148**, 300 (1995).

[12] C. Tsang, IEEE Trans. Magn. **25**, 3692 (1989); C. Tsang and R. Fontana, *ibid.* **18**, 1149 (1982).

[13] B. Dieny, J. Magn. Magn. Mater. **136**, 335 (1994); B. Dieny, V.S. Speriosu, S.S.P. Parkin, B.A. Gurney, D.R. Wilhoit, and D. Mauri, Phys. Rev. B **43**, 1297 (1991).

[14] B.Y. Wong, C. Mitsumata, S. Prakash, D.E. Laughlin, and T. Kobayashi, IEEE Trans. Magn. **32**, 3425 (1996).

[15] H. Kishi, Y. Kitade, Y. Miyake, A. Tanaka, and K. Kobayashi, IEEE Trans. Magn. **32**, 3380 (1996); S. Tadokoro, T. Imagawa, K. Mitsukoya, S. Narishige, S. Soeya, and M. Fuyama, J. Magn. Soc. Jpn. **20**, 357 (1996); S. Soeya, H. Hoshiya, and M. Fuyama, J. Appl. Phys. **80**, 1006 (1996).

[16] J.H. Greiner, J. Appl. Phys. **37**, 1474 (1966).

[17] N. Smith and W.C. Cain, J. Appl. Phys. **69**, 2471 (1991); W.C. Cain and M.H. Kreyder, *ibid.* **67**, 5722 (1990); P.P. Freitas, J.L. Leal, T.S. Plaskett, and L.V. Melo, *ibid.* **75**, 6480 (1994).

[18] J.W. Stout and S.A. Reed, J. Am. Chem. Soc. **76**, 5279 (1954).

[19] R.A. Erickson, Phys. Rev. **90**, 779 (1953).

[20] M.T. Hutchings, B.D. Rainford, and H.J. Guggenheim, J. Phys. C **3**, 307 (1970).

[21] J. Nogués, D. Lederman, T.J. Moran, Ivan. K. Schuller, and K.V. Rao, Appl. Phys. Lett. **68**, 3186 (1996).

[22] Ivan K. Schuller, Phys. Rev. Lett. **44**, 1597 (1980); W. Sevenhans, M. Gijs, Y. Bruynseraede, H. Homma, and Ivan K. Schuller, Phys. Rev. B **34**, 5955 (1986); E.E. Fullerton, Ivan K. Schuller, H. Vanderstraeten, and Y. Bruynseraede, *ibid.* **45**, 9292 (1992).

[23] B. Vidal and P. Vincent, Appl. Opt. **23**, 1794 (1984).

[24] S.K. Sinha, E.B. Sirota, S. Garoff, and H.B. Stanley, Phys. Rev. B **38**, 2297 (1988).

[25] V. Jaccarino, A.R. King, D. Lederman, M. Lui, and C. A. Ramos, *Heteroepitaxy of Dissimilar Materials* edited by R.F.C. Farrow *et al.*, MRS Symposia Proceedings No. 221 (Materials Research Society, Pittsburgh, 1991), p. 3.

[26] T.J. Moran, Ph.D. thesis, University of California San Diego, 1995.

[27] A.S. Borovik-Romanov, Sov. Phys. JETP **11**, 786 (1960); J. Kushauer, C. Binek, and W. Kleemann, J. Appl. Phys. **75**, 5856 (1994); M. Chirwa, L. Lundgren, P. Nordblad, and O. Beckman, J. Magn. Magn. Mater. **15-18**, 457 (1980).

[28] A.P. Malozemoff, Phys. Rev. B **35**, 3679 (1987); A.P. Malozemoff, *ibid.* **37**, 7673 (1988); A.P. Malozemoff, J. Appl. Phys. **63**, 3874 (1988).

[29] D. Mauri, H.C. Siegmann, and P.S. Bagus, J. Appl. Phys. **62**, 3047 (1987).

[30] J. Nogués, D. Lederman, T.J. Moran, and Ivan. K. Schuller, Phys. Rev. Lett. **76**, 4624 (1996).

[31] J. Nogués (unpublished).

[32] T.J. Moran, J. Nogués, D. Lederman, and Ivan K. Schuller, Appl. Phys. Lett. **72**, 617 (1998).

[33] Y. Ijiri, J.A. Borchers, R.W. Erwin, S.H. Lee, P.J. van der Zaag, and R.M. Wolf, Phys. Rev. Lett. **80**, 608 (1998); J. Appl. Phys. **83**, 6882 (1998).

[34] J.A. Borchers, Y. Ijiri, S.H. Lee, C.F. Majkrzak, G.P. Felcher, K.

Takano, R.H. Kodama, and A.E. Berkowitz, J. Appl. Phys. **83**, 7219 (1998).
[35] N.C. Koon, Phys. Rev. Lett. **78**, 4865 (1997).
[36] A.S. Pavlovic, *Thermal Expansion*, edited by D.C. Larsen (Plenum, New York, 1982), Vol. 7, p. 29.
[37] H. Suhl and I.K. Schuller, Phys. Rev. B **58**, 258 (1998).
[38] K. Takano, R.H. Kodama, A.E. Berkowitz, W. Cao, and G. Thomas, Phys. Rev. Lett. **79**, 1130 (1997).
[39] R. Ramírez, M. Kiwi, and D. Lederman, Bull. Am. Phys. Soc. **42**, 445 (1997).